Bias voltage induced *n*- to *p*-type transition in epitaxial bilayer graphene on SiC

Yufeng Guo,[1,2,*] Wanlin Guo,[1,2,†] and Changfeng Chen[2,‡]
[1]*Institute of Nanoscience, Nanjing University of Aeronautics and Astronautics, Nanjing 210016, China*
[2]*Department of Physics and High Pressure Science and Engineering Center, University of Nevada, Las Vegas, Nevada 89154, USA*
(Received 17 May 2009; revised manuscript received 10 July 2009; published 19 August 2009)

We show by extensive first-principles calculations that an *n*- to *p*-type transition in epitaxial bilayer graphene can be induced by applying bias voltage on C-terminated SiC substrate, but cannot occur on Si-terminated SiC. Bias voltage can cause enough charge transfer between top and bottom graphene layers on C-terminated SiC to shift the Dirac level below or above the Fermi level. On both C- and Si-terminated SiC, change in interlayer spacing of the epitaxial bilayer graphene produces charge redistribution that leads to large increase in the energy gap, but cannot raise the Dirac level efficiently. The surface terminated condition or properties of substrate are of essential importance in possible gate tuning electronic behavior of epitaxial graphene on it.

DOI: 10.1103/PhysRevB.80.085424 PACS number(s): 73.20.−r, 71.15.Mb, 73.40.Ns, 81.05.Uw

Graphene systems attract considerable scientific interest for their intriguing properties.[1–5] Both free-standing single-layer and bilayer graphene have zero-gap, and the π-orbitals orthogonal to the graphene planes are responsible for their characteristic electronic properties. A controllable energy gap in bilayer graphene can be opened up by a bias electric field,[6–9] and the field-induced gap can be effectively modulated by adjusting interlayer spacing.[10] When epitaxially grown on a substrate, as in most device applications, graphene systems exhibit new behaviors due to the interactions with substrate. The first or bottom graphene sheet bonds strongly with substrate via hybridization of its π orbitals with the dangling bond states from substrate surface atoms, which is believed to render it electronically inactive.[5,11–15] The intrinsic properties of graphene are recovered by the second graphene sheet.

Unlike its free-standing counterpart, the top layer of epitaxial bilayer graphene in most cases is *n*-type doped by charge transfer which is generally thought to come from substrate, while weak interlayer interaction with the bottom layer can open a small gap at the Dirac point of the top layer.[5,11,12,14] For the application of epitaxial graphene, it is important to realize a controllable adjustment on its properties. A recent experiment shows that epitaxial bilayer graphene on SiC exhibits an *n*-type and *p*-type transition under a top-gated bias, but the underlying mechanism remains unclear.[16] Other experiment and theoretical works report that interlayer conductance of epitaxial bilayer graphene system and interlayer friction of graphene sheets can be tuned by compressing interlayer distance of graphene layers.[13,17] Electric and mechanical methods become an effective and feasible way to modify graphene system properties. However, the physical mechanism for the *n*- to *p*-type transition of graphene layers on substrates and its robust to mechanical deformation is a crucial prerequisite and open challenge for viable applications.

In this study, we show by density functional theory (DFT) calculations that the field-driven *n*- to *p*-type transition in epitaxial bilayer graphene can be realized at the top graphene sheet on C-terminated SiC (C-SiC), but no such transition occurs on Si-terminated SiC (Si-SiC). In contrast, reducing the interlayer spacing between the top graphene and its bottom layer via nanomechanical compression cannot effectively change the doping state on the top graphene, but significantly changes the Fermi level of the top graphene sheet and leads to considerable increase in the energy gap on both C-SiC and Si-SiC. We find that charge transfer and redistribution induced by electric field or nanomechanical tuning display strong dependence on the interface with the substrate and occur between the top and bottom graphene layers, which are the main driving force for changes in the electronic structure of the top graphene sheet.

We have chosen a 6-layer $\sqrt{3}\times\sqrt{3}R30°$ 6H-SiC (0001) or $(000\bar{1})$ cell as the substrate, with its top terminated by Si or C atoms and its bottom terminated by hydrogen atoms. A (2×2) bilayer graphene cell with AB stacking sits on top of the substrate. The computations were performed using the VASP code with the ultrasoft pseudopotential and local density approximation (LDA) for the exchange-correlation potential.[18–20] An energy cutoff of 400 eV and special *k* points sampled on a $7\times7\times1$ Monkhorst-Pack mesh[21] are used to ensure an energy convergence of less than 1 meV/atom. In the periodic supercell, there is a vacuum region larger than 1.6 nm in the direction perpendicular to the graphene planes to avoid any self-interaction of the slabs. External electric field E_{ext} is modeled by adding a sawtooth-like potential along the direction perpendicular to the graphene planes.[22] For each case, the whole system is relaxed by the conjugate-gradient algorithm until the force on each atom is less than 0.1 eV/nm.

Our fully relaxed structure shows that the first (or bottom) layer of bilayer graphene bonds strongly with SiC substrate and behaves as a buffer layer, consistent with previous reports.[11,12] The equilibrium interlayer distances between the top graphene and the bottom layer on Si- and C-SiC are 0.33 and 0.34 nm, respectively. The mismatch between bilayer graphene and SiC substrate lattice leads to an 8% stretch of the graphene cell. The in-plane deformation in the second carbon layer is artificial. Our calculations show that the expansion of the top graphene cell would not result in any qualitative changes. The lattice mismatch induced structural expansion imposes only minor influence on the behaviors of the π bands. Recent experiment shows that the C-face graphene is found in turbostratic phase.[23] Our model cannot describe this case but the discussion about the effects of elec-

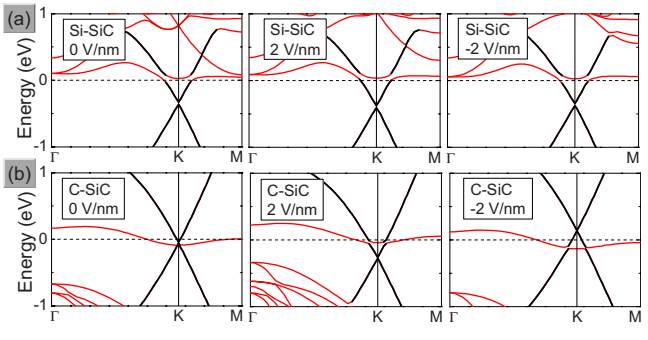

FIG. 1. (Color online) Band structures of bilayer graphene on (a) Si- and (b) C-terminated SiC substrates in the presence of electric fields. The top graphene energy bands are highlighted by dark lines. The Fermi level is set to zero.

tric field and interlayer compression should remain valid.

Figure 1 shows the calculated energy band structures of bilayer graphene of the top graphene layer in the presence of electric fields. On Si-SiC, the Fermi level of the top graphene in the absence of an electric field locates at 0.33 eV above the conical point (the Dirac level), resulting in an *n*-type doping in the graphene. The energy band structures shown in Fig. 1 coincide with previous theoretical results of the same graphene cell on SiC.[11,12] The calculated results show that electric field only has a slight influence on the energy band of the top graphene on Si-SiC. In contrast, the Fermi level of the top graphene on C-SiC is significantly shifted by electric field. The top graphene on C-SiC in the absence of an electric field is approximately neutral [see Fig. 1(b)]. When an electric field of 2 V/nm is applied, the Fermi level of the top graphene locates at 0.26 eV above the Dirac level, indicating an *n*-type transition; however, at −2 V/nm the Dirac level moves above the Fermi level to 0.14 eV so that the top graphene becomes *p* type.

To obtain a better understanding about the effects of electric field, the projected density of states (pDOS) of the top and bottom layers are given in Figs. 2(a) and 2(b), respectively. On Si-SiC, both pDOS of the top and bottom graphene are slightly affected by electric field. On the contrary, an obvious shift in the Fermi level of the top graphene on C-SiC can be seen in the pDOS shown in Fig. 2(a), but

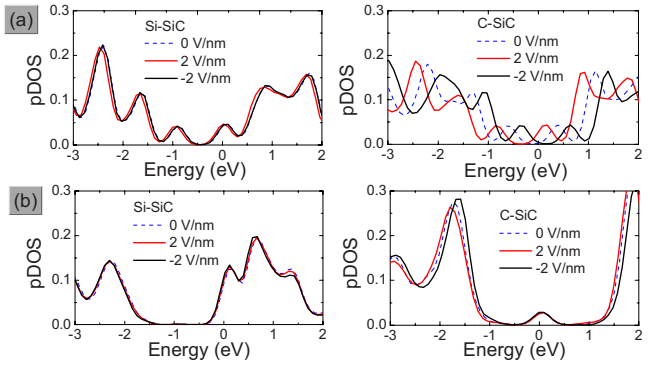

FIG. 2. (Color online) Projected density of states (pDOS) of (a) the top graphene and (b) the bottom graphene layer on SiC (in unit of states/atom). The Fermi level is set to zero.

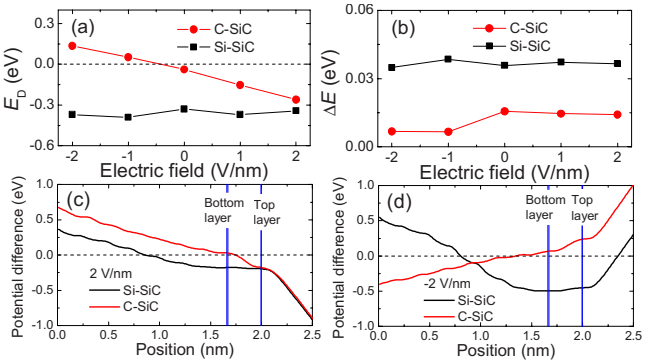

FIG. 3. (Color online) The variations of (a) the Dirac level E_D and (b) energy gap ΔE of the top graphene on SiC in the presence of electric fields. The Fermi level is set to zero. The average electrostatic potential difference between biased and unbiased bilayer graphene along the electric field direction, under (c) 2 V/nm and (d) −2 V/nm. To clarify the electrostatic potential change on the bilayer graphene, only a part of the supercell along the z direction is shown.

not happens at the bottom layer. These results demonstrate that the electron doping to the top graphene is more sensitive to external electric field on C-SiC. Figures 1 and 2 show that applied electric field just shifts the Fermi level without altering the energy band structures of the top graphene, suggesting that a rigid-band model would provide a good description.

The results in Figs. 3(a) and 3(b) show the systematic trends in the variations of the Dirac level E_D and band gap of the top graphene at different electric fields. On C-SiC, the change of electric field from −2 V/nm to 2 V/nm has a remarkable influence on the Dirac level that decreases from 0.14 to −0.26 eV, indicating a *p*- to *n*-type transition. This is in sharp contrast to the situation on Si-SiC where the change in Dirac level is slight and the graphene remains in *n*-type doping. The results also show that the effect of external electric field on the energy gap of the graphene on both Si- and C-SiC substrates is very week, less than 0.01 eV.

Figures 3(c) and 3(d) plot the average electrostatic potential difference between biased and unbiased bilayer graphene along the electric field direction. For 2 V/nm on Si-SiC, the average electrostatic potentials of the top and bottom layers are decreased by the electric field. For C-SiC, the positive electric field decreases the electrostatic potential on the top layer as well, but slightly changes that on the bottom layer, as shown in Fig. 3(c). When an electric field of −2 V/nm is applied, the electrostatic potentials further drop at the top and bottom layers on Si-SiC. In contrast, the electrostatic potential of the top graphene on C-SiC is increased, but the potential on the bottom graphene is still slightly affected [Fig. 3(d)]. It can be seen from these results that the effects of electric field on the epitaxial bilayer graphene strongly depend on the SiC surface termination condition and the interface formed at the bottom graphene layer. The biased top graphene on C-SiC displays a stronger screen effect on its bottom layer than that on Si-SiC.

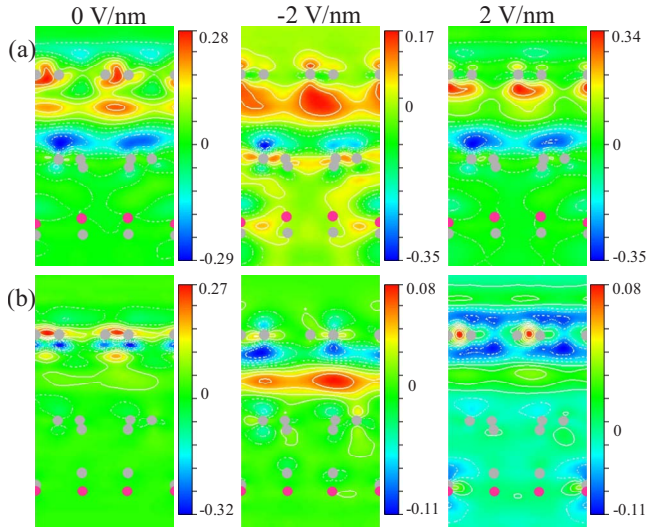

FIG. 4. (Color online) Contour plots of 2D projection of charge density change onto (100) plane in the presence of electric fields. (a) On Si-terminated SiC substrate, (b) C-terminated SiC substrate. The purple atoms in (a) and (b) denote the Si atoms, and the gray atoms denote the C atoms. Contour lines are represented in solid lines for positive values and in broken lines for negative ones, and the largest positive and negative values of the contour lines [in units of $e/(\text{Å})^3$] are shown in each panel. The contour step is set to 1/10 of the range in each case.

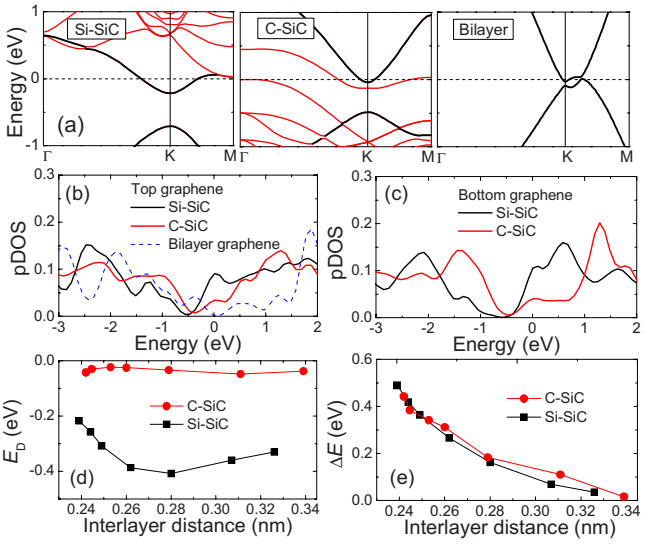

FIG. 5. (Color online) (a) Band structures of the bilayer graphene compressed to an interlayer distance of 0.24 nm on SiC, and the free-standing bilayer graphene with an interlayer distance of 0.24 nm. The top graphene energy bands on SiC are highlighted by dark lines. (b) Projected density of states (pDOS) of the top graphene on SiC and the free-standing bilayer graphene with an interlayer distance of 0.24 nm. (c) Corresponding pDOS of the bottom graphene layer on SiC (in unit of states/atom). The variations of (d) the Dirac level E_D and (e) energy gap ΔE of the top graphene on SiC with interlayer distance. The Fermi level is set to zero.

Figure 4 shows the contour plots of the charge density difference $\Delta\rho^{\text{ext}}=\rho^{\text{ext}}_{\text{tot}}-\rho^{\text{ext}}_{\text{sub+buff}}-\rho^{\text{ext}}_{\text{grap}}$, where $\rho^{\text{ext}}_{\text{tot}}$ is the total charge density in the presence of the vertical electric field, $\rho^{\text{ext}}_{\text{sub+buff}}$ is the charge density of isolated substrate and bottom layer, and $\rho^{\text{ext}}_{\text{grap}}$ is the charge density of isolated top graphene. As different covalent bonds formed between the bottom layer and substrate surface atoms,[11,12] the electron doping state on the top graphene layer on Si-SiC is quite different from that on C-SiC. In the absence of an electric field, there is a lot of accumulated charges in the top graphene on Si-SiC, while charge depletion is concentrated near the bottom layer, as shown in Fig. 4(a). It shows that the charge accumulation for the *n* doping of the top graphene on Si-SiC comes from the bottom layer, rather than from the substrate. On C-SiC, the charge depletion and accumulation are both localized on the top graphene [Fig. 4(b)] so that the graphene remains approximately neutral. The charge distribution gives a clearer explanation to the *n*-type doping and neutral state observed for the top graphene on Si and C-terminated SiC.

A bias electric field of −2 V/nm applied on Si-SiC drives an overall charge transfer between the top and bottom layer [Fig. 4(a)]; but the top graphene layer remains its *n*-doping character (see Fig. 1). The resulting change in charge distribution leads to a slight modification on the Dirac level and a decrease on the electrostatic potential of top graphene [Fig. 3(d)]. For C-SiC under the −2 V/nm bias field, much more pronounced charge transfer from the top graphene to the interior space near the bottom layer occurs, which increases the electrostatic potential [Fig. 3(d)] and causes a transition to *p*-type doping. Reversing the bias field to 2 V/nm leads to additional charge transfer (compared to the unbiased case) from the bottom layer to top graphene on Si-SiC. Interestingly, the charge transfer is confined between the bottom and top graphene layers with little participation from the substrate. This screen effect of the bottom layer limits the charge supply, resulting in only minor changes in the behavior of the top graphene. Meanwhile, C-SiC under 2 V/nm bias field behaves differently in that the majority of charge redistribution occurs near the top graphene layer. There is, however, a small amount of charge transfer from the substrate, rendering the top graphene in *n*-type doping. On biased C-SiC, the charge change on the bottom layer is relatively small and rare as shown by Fig. 4(b), indicating the small influence from the electric field. This also gives an explanation to the results in Figs. 3(c) and 3(d) that the electrostatic potential on the bottom layer is slightly changed by external electric field on C-SiC. The different responses of top graphene to bias field on C-SiC and Si-SiC are rooted in the differences of the covalent and dangling bonds at the interface formed between the bottom graphene layer and the substrate.[11,12] Overall, the field-induced charge transfer, which is vital to the electronic structure modification, mainly occurs between the top graphene and its bottom layer.

We now turn to mechanical tuning of the bilayer graphene on SiC. Figure 5(a) shows the band structures of the bilayer graphene with a compressed interlayer distance of $d=0.24$ nm between the top layer and its bottom layer. For comparison, the band structure of the free-standing bilayer graphene of $d=0.24$ nm is also shown in Fig. 5(a). Both on Si- and C-SiC, the energy bands of the top graphene are obviously deformed, and an energy gap is opened up by the stronger interlayer interaction. The compressed free-standing bilayer graphene shows a cone split around the Fermi level,

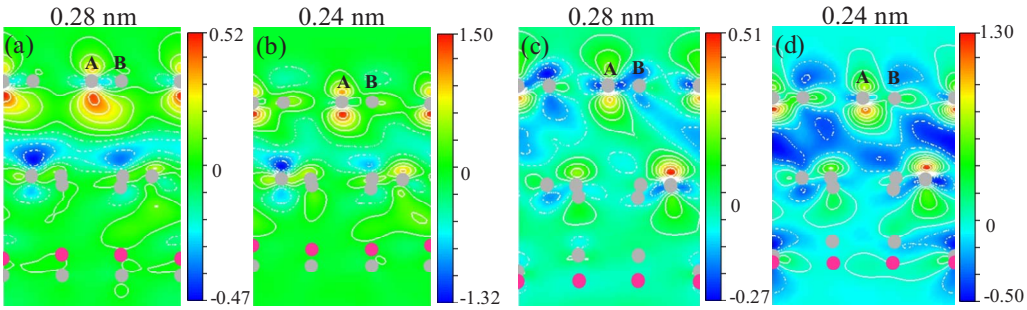

FIG. 6. (Color online) Contour plots of 2D projection of charge density difference onto (100) plane with compression of interlayer distance. (a) (b) On Si-SiC, (c) (d) C-SiC. The notations are the same as in Fig. 4.

but it is still metallic. The corresponding pDOS of the top and bottom graphene are shown in Figs. 5(b) and 5(c). After compressed, the calculated pDOS of the bilayer graphene are significantly altered from its initial state (Fig. 2). Comparing Figs. 5(b) and 5(c), it suggests substantial changes of the π bands and interlayer bonding between top and bottom graphene. On the other hand, the interaction between epitaxial top and bottom graphene layers is quite different from the isolated bilayer graphene because of bonding states of bottom layer with the substrate.

Figure 5(d) plots the variations of the Dirac level E_D of the top graphene with compressed interlayer distance d. On C-SiC, E_D remains insensitive to d down to 0.24 nm. On Si-SiC, E_D decreases until the interlayer distance reduces 0.28 nm, and then increases with further compressing d. Meanwhile, the energy gaps of the top graphene on both Si- and C-SiC increase monotonically with reducing interlayer distance, as shown in Fig. 5(e). The doping states on the top graphene are not effectively influenced on both Si- and C-SiC, although compressing interlayer distance significantly changes the band structure and energy gap of the top graphene in both cases.

We present in Fig. 6 the charge density difference $\Delta\rho$ in response to compression of the interlayer distance. Here $\Delta\rho=\rho_{\text{tot}}-\rho_{\text{sub+buff}}-\rho_{\text{grap}}$, ρ_{tot} is the total charge density of the system, $\rho_{\text{sub+buff}}$ is the charge density of isolated substrate and bottom layer, and ρ_{grap} is the charge density of isolated top graphene at the corresponding position. When interlayer distance decreases to 0.28 nm [Figs. 6(a) and 6(c)], the charge accumulation becomes more localized and intense at the A site of the top graphene on SiC substrate, and no accumulated charge is observed at the B site. The symmetry at the A and B sites is thus broken by the charge redistribution and this leads to the opening of an energy gap. The gap increases with further compression of the interlayer distance to 0.24 nm [Figs. 6(b) and 6(d)], signaling the stronger effect of the symmetry breaking. At the interlayer distance of 0.24 nm, the charge accumulation at the top graphene on Si-SiC is more concentrated, as shown in Fig. 6(b). On the contrary, the distribution of accumulated charge on C-SiC is similar to that at 0.28 nm [Fig. 6(d)]. This explains the increase in the Dirac level on Si-SiC [Fig. 5(d)] for interlayer distance below 0.28 nm. Similar to effects induced by electric field, mechanical tuning induced charge accumulation and depletion mainly occur between the top graphene and its bottom layer.

To further understand the interface effect on the symmetry at the A and B sites, Fig. 7 shows contour plots of two-dimension (2D) profile (001) of charge density difference at the top graphene. For Si-SiC with an equilibrium interlayer distance, the charge distribution at the A site is slightly different from that at the B site [Fig. 7(a)]. This leads to the cone splitting and a small energy gap opened up. The symmetry at the A and B sites is almost not affected for the equilibrium top graphene on C-SiC [Fig. 7(c)] so that the cone splitting is much smaller as shown by Fig. 3(b). When the interlayer distance is compressed to 0.24 nm, the symmetry is obviously broken at the A and B sites on both Si- and C-SiC [Fig. 7(b) and 7(d)]. The bottom graphene layer imposes a stronger influence on the charge distribution of the top graphene.

In summary, we demonstrate by DFT calculations that the interface formed between the bottom layer of epitaxial bilayer graphene on SiC and the substrate surface condition play a key role in tuning the properties of the top graphene that is subjected to bias electric fields or interlayer spacing compression. The n- to p-type transition can only occur on carbon terminated SiC under bias voltage. Nanomechanical compression cannot efficiently change the doping state of top graphene. Charge redistribution and transfer between the top and bottom layers are identified as the driving mechanism for the field induced transition of doping state and the gap variation tuned by interlayer spacing compression. Our results

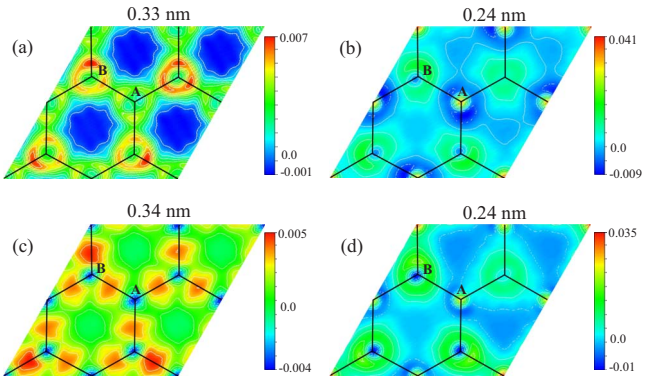

FIG. 7. (Color online) Contour plots of 2D profile (001) of charge density difference at the top graphene. (a) (b) On the Si-SiC with an interlayer distance of 0.33 and 0.24 nm, (c) (d) on the C-SiC with an interlayer distance of 0.34 and 0.24 nm. Other notations are the same as in Fig. 4.

provide insights for fundamental understanding of epitaxial graphene under electric field and mechanical tuning and, in particular, suggest a mechanism for gate-bias induced *n*- to *p*-type transition that has been observed in recent experiments.

This work is supported by DOE Cooperative Agreement DE-FC52-06NA26274 at UNLV, the 973 Program (Grant No. 2007CB936204), NSF (Grant No. 10732040), MOE (Grant No. 705021,IRT0534) of China at NUAA, and Innovation Fund of NUAA.

*yfguo@physics.unlv.edu
†wlguo@nuaa.edu.cn
‡chen@physics.unlv.edu

[1] K. S. Novoselov, A. K. Geim, S. V. Morozov, D. Jiang, Y. Zhang, S. V. Dubonos, I. V. Grigorieva, and A. A. Firsov, Science **306**, 666 (2004).
[2] A. K. Geim and K. S. Novoselov, Nature Mater. **6**, 183 (2007).
[3] E. McCann and V. I. Fal'ko, Phys. Rev. Lett. **96**, 086805 (2006).
[4] J. Nilsson, A. H. Castro Neto, F. Guinea, and N. M. R. Peres, Phys. Rev. Lett. **97**, 266801 (2006).
[5] S. Y. Zhou, G.-H. Gweon, A. V. Fedorov, P. N. First, W. A. de Heer, D.-H. Lee, F. Guinea, A. H. Castro Neto, and A. Lanzara, Nature Mater. **6**, 770 (2007).
[6] E. V. Castro, K. S. Novoselov, S. V. Morozov, N. M. R. Peres, J. M. B. Lopes dos Santos, J. Nilsson, F. Guinea, A. K. Geim, and A. H. Castro Neto, Phys. Rev. Lett. **99**, 216802 (2007).
[7] T. Ohta, A. Bostwick, T. Seyller, K. Horn, and E. Rotenberg, Science **313**, 951 (2006).
[8] F. Guinea, A. H. Castro Neto, and N. M. R. Peres, Phys. Rev. B **73**, 245426 (2006).
[9] H. Min, B. Sahu, S. K. Banerjee, and A. H. MacDonald, Phys. Rev. B **75**, 155115 (2007).
[10] Y. F. Guo, W. L. Guo, and C. F. Chen, Appl. Phys. Lett. **92**, 243101 (2008).
[11] A. Mattausch and O. Pankratov, Phys. Rev. Lett. **99**, 076802 (2007).
[12] F. Varchon, R. Feng, J. Hass, X. Li, B. Ngoc Nguyen, C. Naud, P. Mallet, J.-Y. Veuillen, C. Berger, E. H. Conrad, and L. Magaud, Phys. Rev. Lett. **99**, 126805 (2007).
[13] P. W. Sutter, J. Flege, and E. A. Sutter, Nature Mater. **7**, 406 (2008).
[14] S. Kim, J. Ihm, H. J. Choi, and Y. W. Son, Phys. Rev. Lett. **100**, 176802 (2008).
[15] D. Martoccia, P. R. Willmott, T. Brugger, M. Björck, S. Günther, C. M. Schlepütz, A. Cervellino, S. A. Pauli, B. D. Patterson, S. Marchini, J. Wintterlin, W. Moritz, and T. Greber, Phys. Rev. Lett. **101**, 126102 (2008).
[16] Y. Q. Wu, P. D. Ye, M. A. Capano, Y. Xuan, Y. Sui, M. Qi, J. A. Cooper, T. Shen, D. Pandey, G. Prakash, and R. Reifenberger, Appl. Phys. Lett. **92**, 092102 (2008).
[17] Y. F. Guo, W. L. Guo, and C. F. Chen, Phys. Rev. B **76**, 155429 (2007).
[18] G. Kresse and J. Hafner, Phys. Rev. B **47**, 558 (1993).
[19] G. Kresse and J. Hafner, Phys. Rev. B **49**, 14251 (1994).
[20] D. Vanderbilt, Phys. Rev. B **41**, 7892 (1990).
[21] H. J. Monkhorst and J. D. Pack, Phys. Rev. B **13**, 5188 (1976).
[22] J. Neugebauer and M. Scheffler, Phys. Rev. B **46**, 16067 (1992).
[23] K. V. Emtsev, F. Speck, Th. Seyller, L. Ley, and J. D. Riley, Phys. Rev. B **77**, 155303 (2008).